CHAPTER-3

Spectral Analysis

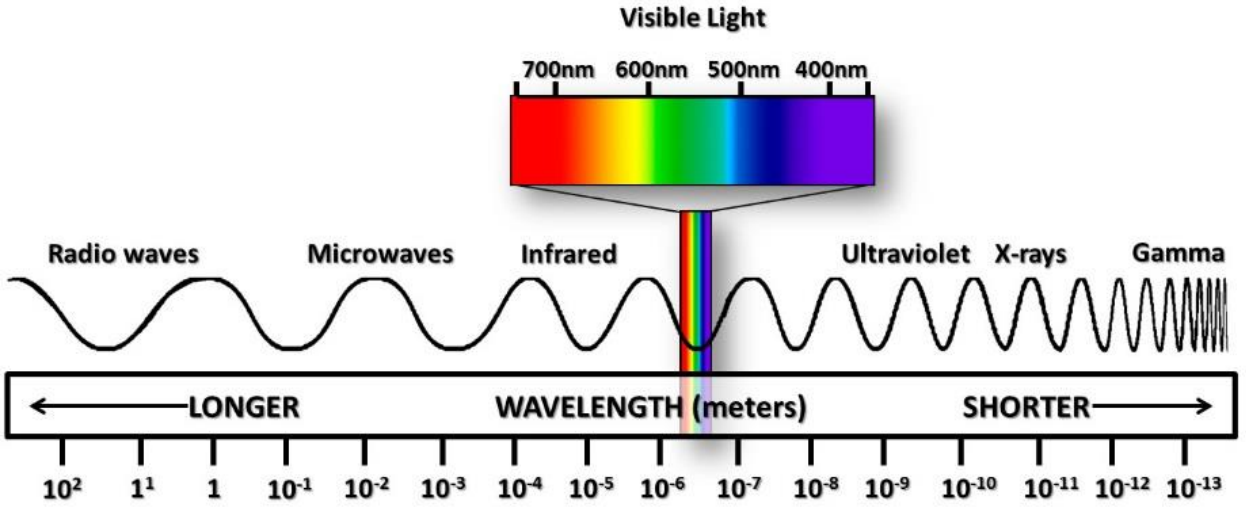

INSTRUMENTAL TECHNIQUES

The characteristics of adsorbents have a great influence on their adsorption performances. Hence, the characterization of any synthesized adsorbent is very important in order to fully understand its adsorption performance in an adsorbent-adsorbate interaction.

The native BFA and the synthesized adsorbents CaFZBFA, MgFZBFA, CaMZBFA and MgMZBFA were characterized by different spectral techniques. The elemental composition was determined by X-ray fluorescence (XRF) technique. The mineralogical characterizations of the adsorbents were carried out with the help of wide-angle Powder X-ray Diffraction (PXRD) technique. Microscopic evaluation was done by Scanning Electron Microscopy (SEM) technique. Fourier Transform Infrared Spectroscopy (FTIR) was used to characterize the major functional groups present in the synthesized adsorbent materials

❖ X-ray Fluorescence (XRF)

XRF is used for the determination of elemental composition of a wide variety of minerals or materials including solids and liquids. The principle is based on the interaction of X-rays with the electrons of atoms present in a material. Secondary X-rays are generated from these interactions which are characteristic of the constituent elements present in the material.

An X-ray instrument basically contains an X-ray source, the sample compartment and the detector (Figure 3.1). The X-ray source is an X-ray tube, which is a device for generating X-rays by accelerating electrons to high energies and causing them to strike a metal target from which X-rays are emitted.

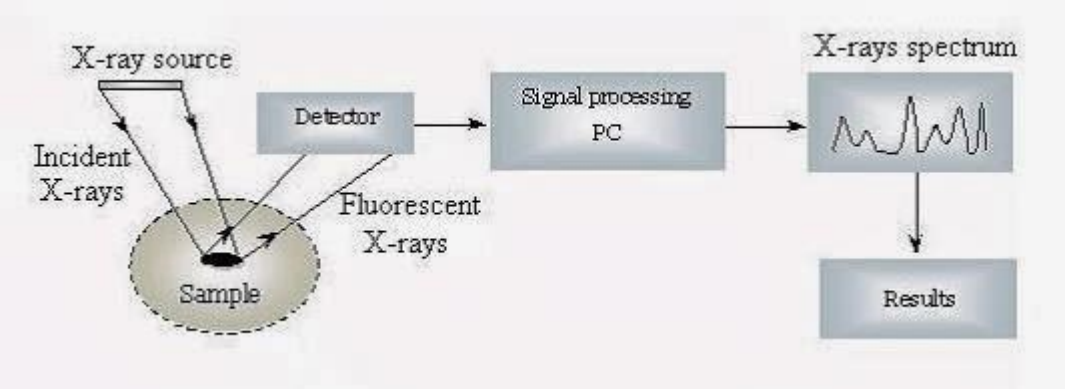

Figure 3.1 Schematic diagram of X-ray fluorescence instrumentation and technique

Primary X-rays are generated by the source and directed at the surface of the sample, sometimes passing through a filter to modify the X-ray beam. When the beam hits the atoms in the sample, the atoms react by generating secondary X-rays that are collected and processed by the detector. The reaction between the primary X-rays and an atom after the collision is based on the disturbance of the state of equilibrium of the atom. The disturbance results from the absorption of the electromagnetic radiation by the atoms, transferring all the photon energy to the internal electrons of the constituent atoms. The electrons become excited, gets expelled from their respective inner shells thus creating vacancies. This effect is known as the photo-electric effect. In order to annul the effect of the equilibrium disturbance, an electron from a higher energy level (outer shell) fills the previously created vacancy. The movement of such an electron from a higher energy level (outer shell) to a lower energy level (inner shell) results in the generation of a secondary X-ray which is characteristic of an element. This process of the emission of X-rays is called X-ray fluorescence. The secondary X-rays emitted by the atoms in the sample are collected by the detector and processed in the analyzer to produce information about the constituent atoms present in the sample and the

intensities of a fluoresced X-rays attributed to specific atoms are proportional to the respective quantities or concentrations of the elements [1, 2].

The elemental composition of the raw BFA and the synthesized zeolitic composite adsorbents: CaFZBFA, MgFZBFA, CaMZBFA and MgMZBFA were analysed using XRF instrument PANalytical AxiosMAX Wavelength-Dispersive) at Sophisticated Instrumentation Centre for Applied Research and Testing (SICART), Vidyanagar, Gujarat, India. About 5 – 8 g of the dried and powdered samples were required for the analysis. The sample was pressed into pellets using a hydraulic press meant for the specific purpose prior to the introduction of the samples into the sample compartments.

❖ Powder X-ray Diffraction Spectroscopy (PXRD)

PXRD spectroscopy is an analytical technique used for phase identification of crystalline materials. The materials to be analysed using this technique are usually finely ground and homogenized solids so that the result could be representative of the bulk.

The principle is based on the diffraction of X-rays directed toward a powdered solid sample. The crystalline constituents (having a regular array of atoms) in the sample cause the incident electromagnetic radiation to diffract (through the atoms) into many specific positions at specific angles. The diffracted rays are collected along with their respective diffraction angles, intensities and angles of diffraction and used for the qualitative determination of the mineral phases present in the sample.

A PXRD instrument basically contains an X-ray source, the sample compartment and the detector (Figure 3.2). X-rays are generated from the cathode ray tube, filtered to produce monochromatic radiation, collimated to concentrate and directed toward the sample. The interaction of the X-rays with

the powder sample produces constructive interference (and a diffraction ray) when conditions satisfy Bragg's law ($n\lambda = 2d\sin\theta$). This law relates the wavelength of electromagnetic radiation to the diffraction angle and the lattice spacing in a crystalline sample. The diffracted X-rays are then detected, processed and counted with the help of multichannel analyser.

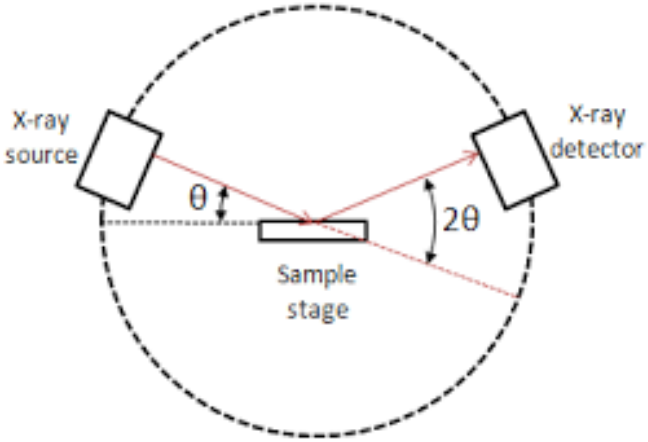

Figure 3.2 Schematic diagram of X-ray diffraction spectroscopy

By scanning the sample through a wide range of 2θ angles, all possible diffraction directions of the lattice should be attained due to the random orientation of the powdered material. The conversion of the diffraction peaks to d-spacings could allow the identification of the materials in the sample because each mineral has a set of unique d-spacings. Typically, this is achieved by the comparison of the d-spacings with standard reference patterns [3].

The PXRD for BFA, CaFZBFA, MgFZBFA, CaMZBFA and MgMZBFA was carried out with a PXRD instrument [Rigaku MiniFlex XRDBD111915 with CuKα radiation (λ = 1.5406 Å) and Ni filter at 40 kV] at Sardar Vallabhbhai National Institute of Technology (SVNIT), Surat, Gujarat, India. About 200 mg of the dried and powdered samples were required for the analysis. The

sample was carefully placed into the sample holder of the instrument, making sure that excess samples were removed from the edges, and the sample holder appropriately placed in the XRD sample slot for the analysis. During the analysis, diffractograms of the samples were recorded over a range of 2θ values from 5° to 90°. The scanning rate was set at 0.0130°/min with continuous scanning.

❖ Fourier Transform Infrared Spectroscopy (FTIR Spectroscopy)

FTIR spectroscopy is a rapid, economical, easy and non-destructive technique for the identification of functional groups present in organic and inorganic samples. The principle of operation is based on the measurement of the interaction of infrared electromagnetic radiation with the sample. Atoms in the functional groups of a typical sample absorb some fraction of the incident infrared radiation that reaches them and causing stretching/bending vibration of the functional group, causing attenuation of the incident radiation at specific frequencies or wavenumbers. The specific frequencies of vibration of the sample are identified with respect to reference functional groups IR vibrational frequencies, and this will suggest the identity of the functional groups present in the sample.

The basic components of an FTIR spectrometer are the IR source, the interferometer, the sample compartment and the detector (Figure 3.3). A polychromatic beam of IR radiation emerges from the source, enters the interferometer where a special pattern of the signal (interferogram) is produced. The resulting beam passes through the sample compartment where it is transmitted through the surface of the sample. The specific frequencies of energy which are unique to the sample are absorbed (and identification is

based on this). The radiation finally passes through the detector which continually monitors the full wavelength range of the IR radiation.

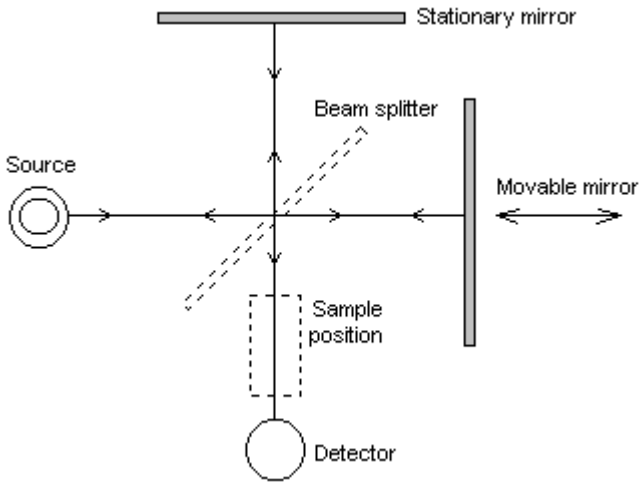

Figure 3.3 Schematic diagram of the operation of FTIR spectrometer

The connected computer finally converts the signals received by the detector into an absorption spectrum (via Fourier transformation) which is peculiar to a particular sample [4].

FTIR spectroscopy utilizes mainly the middle-infrared region (4000 – 300 cm^{-1}) where stretching (υ) and bending vibrations (δ) which are characteristic groups of samples could appear.

The FTIR spectra of BFA, CaFZBFA, MgFZBFA, CaMZBFA and MgMZBFA were obtained using PerkinElmer GX at Sophisticated Instrumentation Centre for Applied Research and Testing (SICART), Vidyanagar, Gujarat, India. Highly purified and desiccated spectroscopic grade 1.0 g KBr and 4 – 5 mg of well-dried sample was mixed thoroughly and ground in a mortar. The finely ground mixture was then transferred to the mould and the pellets prepared in this manner were introduced into the sample chamber of the FTIR spectrometer.

❖ Scanning Electron Microscopy (SEM)

SEM is an analytical technique for investigating the surface topography of a sample. The principle is based on the interaction of a beam of electrons with the surface of the sample which results in the generation of signals that are analysed to give information about surface morphology of the sample of interest.

A typical scanning electron (Figure 3.4) microscope consists of the source of electrons (electron gun), a column down which electrons travel with electromagnetic lenses, the sample chamber and the secondary electrons detector.

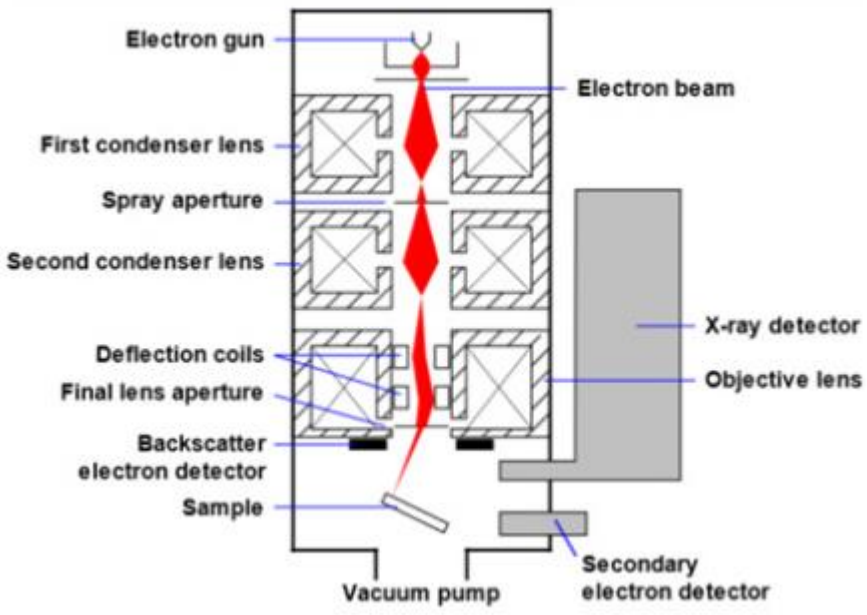

Figure 3.4 Diagrammatic illustration for scanning electron microscope

The electrons produced at the top of the column by an electron gun are accelerated and passed through a combination of lenses and apertures to produce a focused beam of electrons which hits the surface of the sample (in the sample compartment). The electrons beam penetrates the sample to a depth

of few microns, interacts with the sample and characteristic X-rays are generated. The signals are collected by one or more detectors to form images which are displayed on the screen of the attached computer [5].

The SEM images for BFA, CaFZBFA, MgFZBFA, CaMZBFA and MgMZBFA were obtained using FEI Field Emission Gun Nano Nova FEG-SEM 450 with EDAX at Sophisticated Instrumentation Centre for Applied Research and Testing (SICART), Vidyanagar, Gujarat, India. About 100 mg of the dried and powdered samples were introduced into the sample chamber of the instrument, and the SEM images were viewed at suitable magnifications.

RESULTS AND INTERPRETATIONS

The general mechanism for zeolite synthesis from fly ash is basically in three stages which involve:

- The breaking down of aluminium and silicon content of the fly ash
- The dissolution of the silicon and aluminium content and interaction which results in the formation of aluminosilicate gel
- The crystallization of zeolite phases from the aluminosilicate gel.

In the fusion synthesis process, the alkali treatment of the fly ash under the muffle furnace temperature conditions is responsible for the breaking down of the inherent silica and alumina. The stirring in aqueous solution ensures the proper mixing of the reactants and the formation of aluminosilicate gel which results in the nucleation of zeolites. The last stage of the synthesis which is the low-temperature microwave treatment enabled the crystallization of the nucleated zeolites phases.

For the microwave hydrothermal process, the breaking down of silica and alumina; the formation of aluminosilicate gel; the nucleation; and the crystallization of zeolite phases, all take place under a single microwave induced high-temperature alkaline hydrothermal treatment of the fly ash.

❖ X-ray Fluorescence

It can be observed that the BFA has very low alumina content compared to silica (Si/Al is 54.3) (Table 3.1). The relative rise of alumina in CaFZBFA, MgFZBFA, CaMZBFA and MgMZBFA compared to BFA is due to aluminium supplementation by the inclusion of sodium aluminate in the

syntheses. This was done to lower the Si/Al ratio in order to boost the chance for zeolitization.

The dissolution of the components of BFA precedes the formation of aluminosilicate gel which eventually crystallizes as zeolites. It can be observed that the Si/Al ratio of CaFZBFA and MgFZBFA (both obtained by the alkali fusion synthesis method) are significantly lower than those of CaMZBFA and MgMZBFA (both obtained by microwave alkaline hydrothermal synthesis method). This observation suggests that more dissolved silica was available for much Al incorporation during the formation of aluminosilicate gel in the case of the alkali fusion synthesis method than in the case of the alkaline hydrothermal method. This says much about the efficiency of the dissolution of amorphous and crystalline components of the BFA, most especially the silica components, and the chance of zeolitization. It could be inferred that the alkali fusion method that produced CaFZBFA and MgFZBFA were more efficient in terms of breaking down and solubilizing the silica constituents of BFA for zeolitization. Also, the better incorporation of Al in the fusion syntheses than in the hydrothermal syntheses suggests why there is greater incorporation of Ca(II) and Mg(II) in CaFZBFA and MgFZBFA respectively than in CaMZBFA and MgMZBFA. In zeolitization, Al^{3+} being triply charged and replacing some of Si^{4+} in their tetrahedral positions in the aluminosilicate structure results in the deficiency of positive charge which must be balanced in order to attain stability. Therefore, the greater incorporation of Ca(II) and Mg(II) in CaFZBFA and MgFZBFA is because more Al had the chance to be introduced into the zeolitic frameworks or/ and the proportions of zeolite phases in CaFZBFA and MgFZBFA are more than those of the corresponding alkaline hydrothermal products CaMZBFA and MgMZBFA.

Table 3.1 Chemical compositions (by XRF study) of BFA and the adsorbents

Chemical Constituents (%)	BFA	CaFZBFA	MgFZBFA	CaMZBFA	MgMZBFA
SiO_2	83.14	40.37	53.16	68.56	67.64
Al_2O_3	1.53	6.06	11.61	5.35	5.43
Na_2O		2.12	4.39	2.80	2.86
CaO	2.60	37.70	6.32	7.67	1.30
MgO	1.60	0.88	11.62	0.99	6.12
K_2O	4.23	0.55	1.06	5.16	5.21
Cl	0.05				
Fe_2O_3	6.06	4.35	7.39	6.17	6.96
MnO	0.22	0.23	0.22	0.21	0.23
TiO_2	0.29	0.74	0.96	0.84	0.68
SiO_2/Al_2O_3	54.30	6.65	4.57	12.79	12.45

❖ Fourier Transform Infrared Spectroscopy

Fourier Transform Infrared Spectroscopy (FTIR) was used to confirm the zeolitization of BFA. Table 3.2 characterizes the BFA and the synthesized zeolitic composite adsorbents: CaFZBFA; MgFZBFA; CaMZBFA; and MgMZBFA, by their IR absorption vibrations at specific wavenumbers. The IR vibrational spectra (Figure 3.5 – 3.9) show the changes that occur from the starting material BFA to the syntheses products CaFZBFA, MgFZBFA, CaMZBFA and MgMZBFA. The IR absorption bands 1150.85 cm^{-1}, 791.68 cm^{-1} and 473.53 cm^{-1} in BFA spectrum (Figure 3.5) result from the stretching and bending of the internal tetrahedral TO_4 (T = Si, Al) corresponding to the asymmetrical stretching vibrations of Si-O-Si; the symmetrical stretching vibrations of Si-O-Si; and the bending vibrations of O-Si-O respectively [6, 7]. The broad band at 3395 cm^{-1} corresponds to the stretch band of OH group and

this can be associated with adsorbed water. For the synthesized products (Figure 3.6 – 3.9), there is an increase in the intensities in the broad band associated with the stretching OH. This suggests the appearance of Si-OH group which is a feature of a typical zeolite material [8]. Also for the synthesized products, the bands that appear at 1637 cm^{-1} (which is noticeably absent in the spectrum of BFA) are vibrations peculiar to OH functional group which can be ascribed to water of zeolitic nature [9]. In addition, the TO_4 bands in the synthesized products (initially at 1150 cm^{-1} in the spectrum of BFA) have shifted to lower wavenumbers and they appear to be more intense. It has been established that the wavenumber of this asymmetric stretching vibration band decreases with an increase in Al content. Hence, the shift of the T-O band to lower wavenumber indicates the incorporation of Al in the TO_4 of aluminosilicate to increase in the number of tetrahedrally positioned Al to form zeolites [7, 10, 11]. The shift of the asymmetric TO_4 bands to lower wavenumbers is conspicuously more in CaFZBFA and MgFZBFA than in CaMZBFA and MgMZBFA, and this is in absolute agreement with the result from XRF analysis which shows less Si/Al ratio for CaFZBFA and MgFZBFA than CaMZBFA and MgMZBFA. This further emphasises the more efficient breaking down and dissolution of BFA components for zeolitization in CaFZBFA and MgFZBFA than in CaMZBFA and MgMZBFA for the zeolitization process.

Table 3.2 FTIR characterization of BFA, CaFZBFA, MgFZBFA, CaMZBFA, and MgMZBFA

Wavenumber (cm^{-1})	**Possible assignments**	**Observed bands (cm^{-1})**				
		BFA	**CaFZBFA**	**MgFZBFA**	**CaMZBFA**	**MgMZBFA**
3800-3300	Stretching vibration of -OH group, silanol (Si-OH)	3395	3440	3440	3438	3439
1700-1400	OH deformation and bending vibration of interstitial water	-	1638	1640	1638	1638
1250-850	Asymmetric internal T-O stretching of TO_4 tetrahedra, Si-O-Si (T = Si, Al)	1151	1023	1018	1090; 1070; 1024	1091; 1022
800-600	Symmetric stretching of internal tetrahedra TO_4	792	666; 713; 735	750	791	791
420-500	Bending mode of internal tetrahedra TO_4 (O-T-O)	473	441; 446	460	473	473

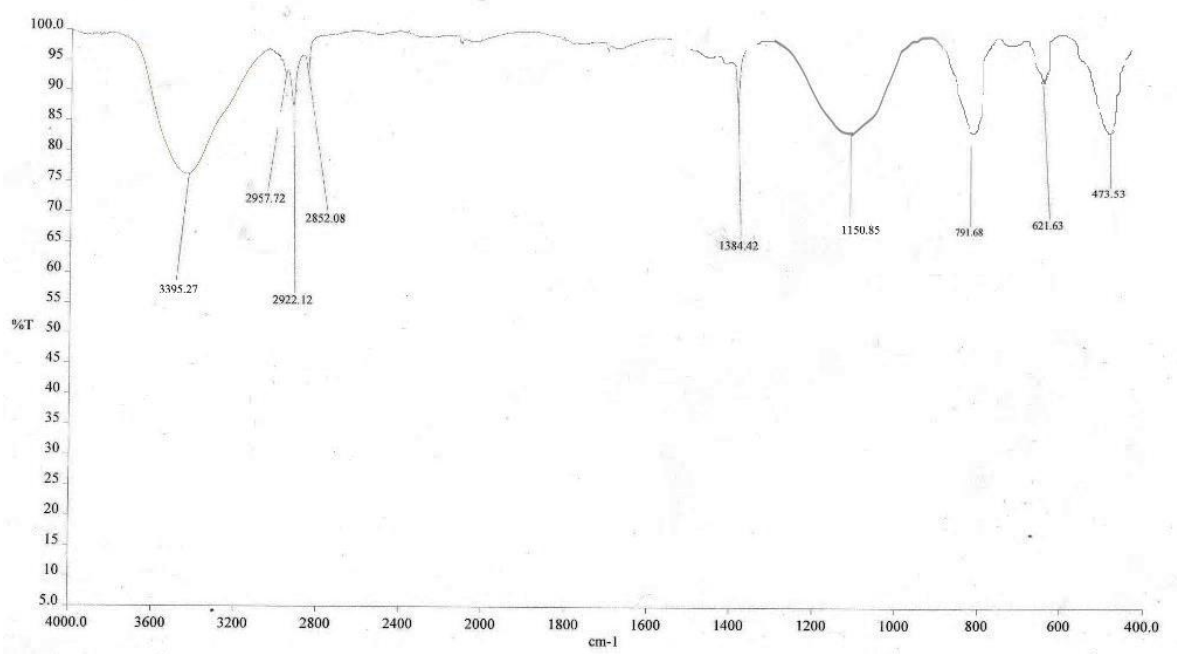

Figure 3.5 FTIR absorption spectrum of BFA

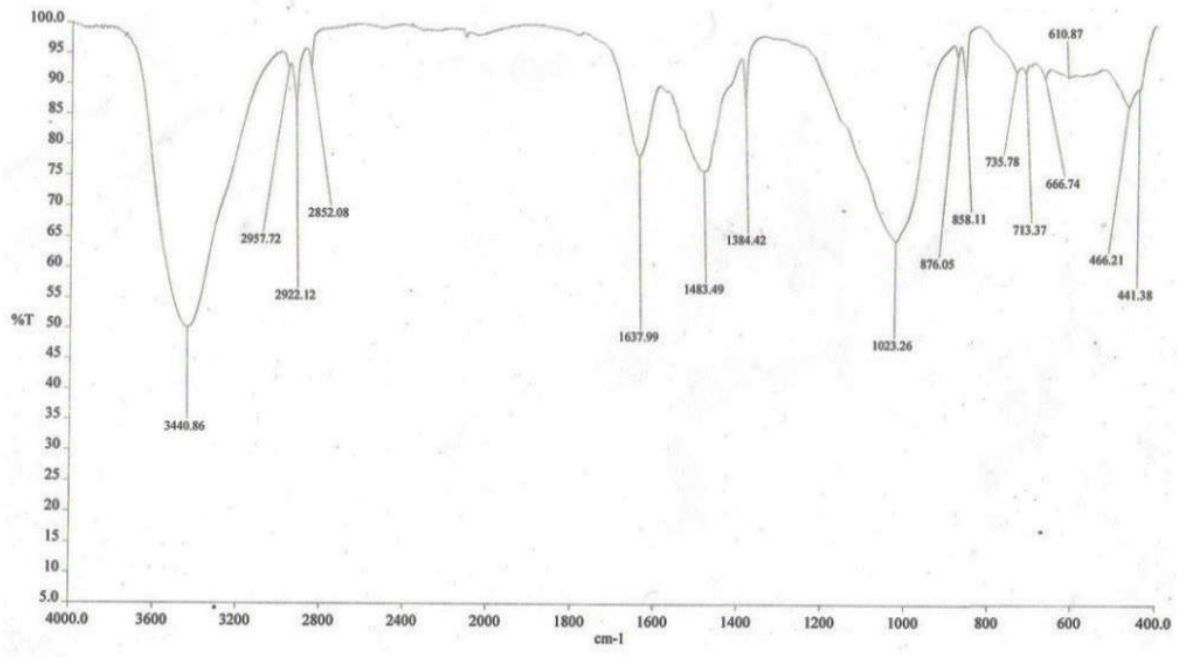

Figure 3.6 FTIR absorption spectrum of CaFZBFA

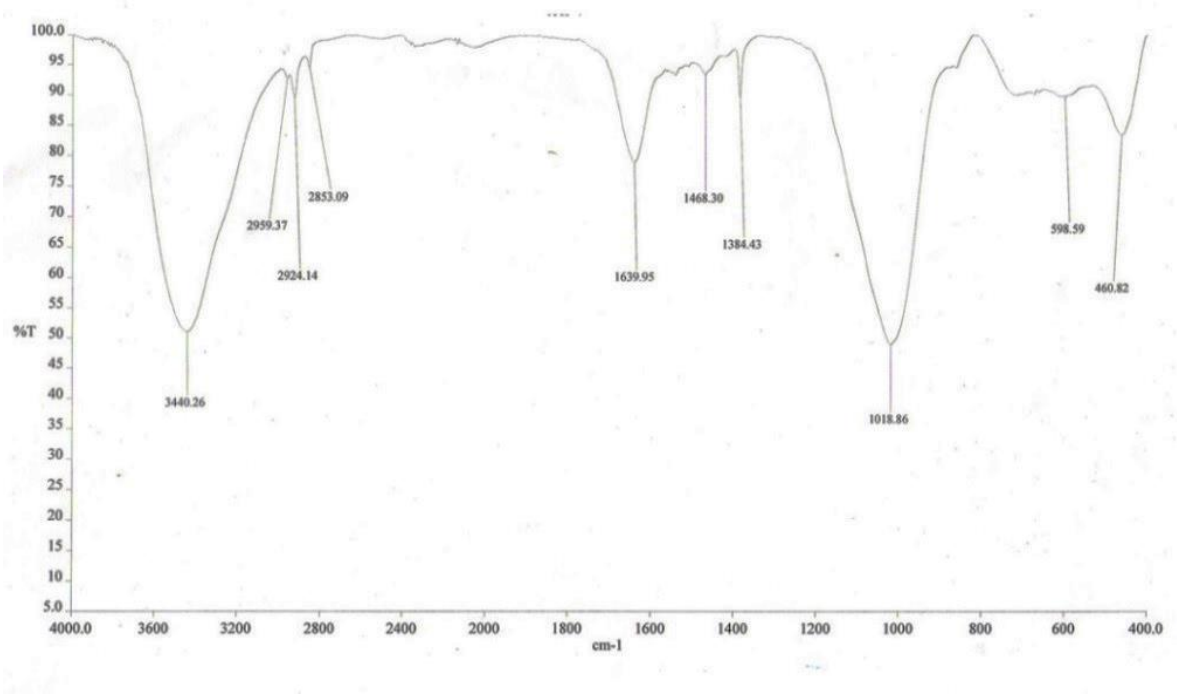

Figure 3.7 FTIR absorption spectrum of MgFZBFA

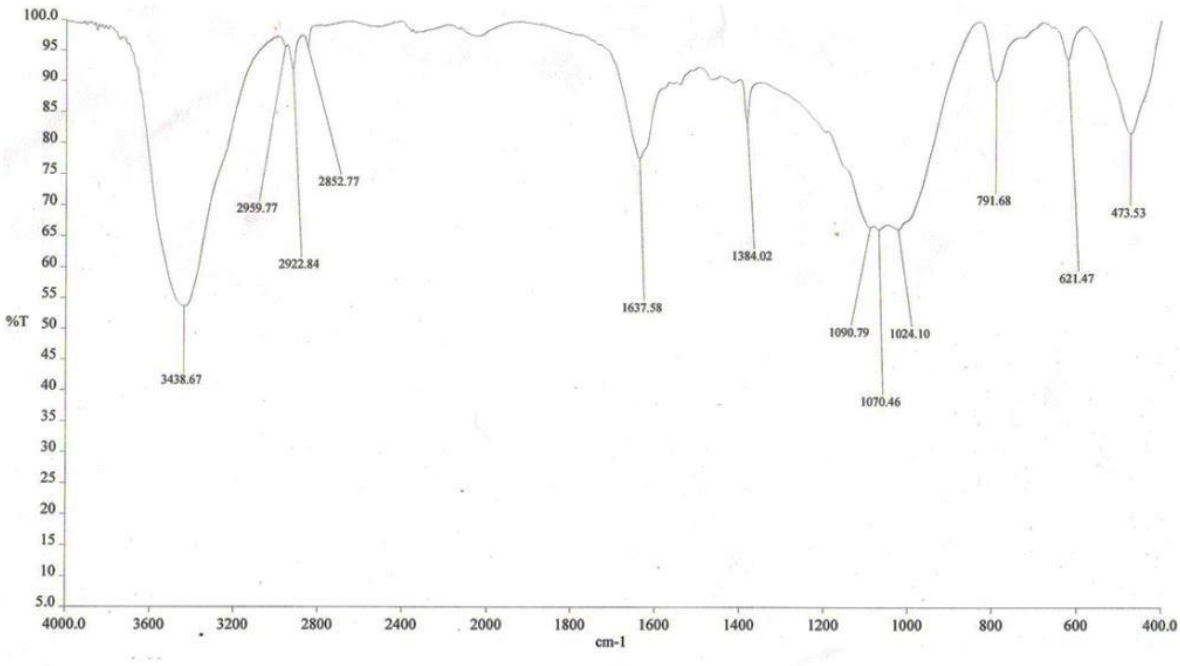

Figure 3.8 FTIR absorption spectrum of CaMZBFA

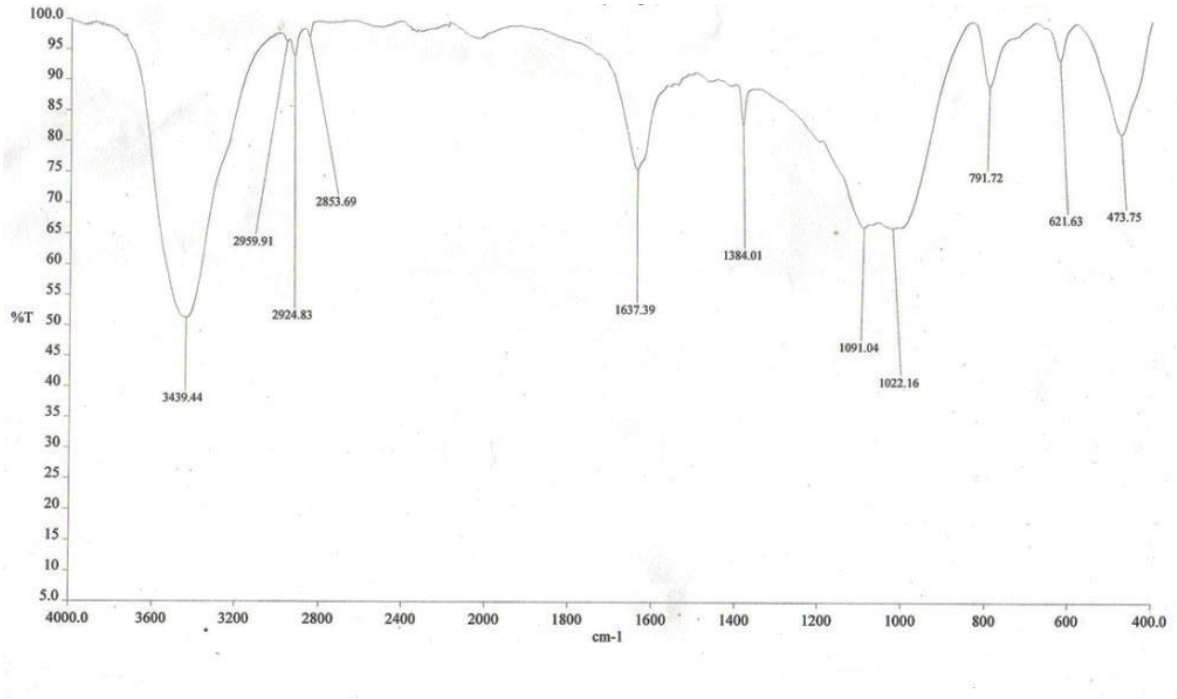

Figure 3.9 FTIR absorption spectrum of MgMZBFA

❖ Powder X-ray diffraction (PXRD)

The PXRD spectra (Figure 3.10 – 3.14) also reflect some changes that occur from the starting material BFA to the syntheses products CaFZBFA, MgFZBFA, CaMZBFA and MgMZBFA. The mineral phases represented by the diffractograms of BFA, CaFZBFA, MgFZBFA, CaMZBFA and MgMZBFA were identified based on Crystallographic Open Database for Inorganic Compounds (COD-Inorg REV198327 2017.07.03) using a software 'Match! Version 2'. The software works by comparing the diffraction patterns of samples with the numerous reference patterns of inorganic phases present in the Crystallographic Open Database and by this, the mineral phases in the samples were identified.

The diffractogram for BFA (Figure 3.10) shows a broad hump ($2\theta = 20 – 40^{o}$) suggests that it contains a substantial amount of glassy amorphous phase. Silicon oxide diffractions such as that of quartz ($2\theta = 20.84^{o}$, 26.64^{o}, 36.5^{o}, 60.08^{o} and 77.68^{o}) and cristobalite ($2\theta = 21.90^{o}$) were, however, detected in the diffractogram. Diffraction attributed to mullite ($2\theta = 42.66^{o}$) was also found.

Judging from the diffractograms of fusion method products CaFZBFA and MgFZBFA (Figures 3.11 and 3.12), fusion method seems to be a very harsh method, as the initial constituents such as quartz, mullite and cristobalite seem almost completely broken down and can rarely be seen in the XRDs of CaFZBFA and MgFZBFA. Furthermore, there is a massive disappearance of the BFA hump and the appearance of entirely new crystalline peaks can be observed. These observations suggest that the BFA had undergone some major transformations during the syntheses process which must have involved the major dissolution of the amorphous and crystalline silica and alumina phases that were present in the BFA into aluminosilicates and crystallization as zeolites. Diffraction peaks of zeolitic composites involving faujasite-Ca ($2\theta = 6.06^{o}$, 10.10^{o}, 29.28^{o} and 31.04^{o}), sodalite ($2\theta = 13.98^{o}$, 21.90^{o}, 24.36^{o} and 47.42^{o}) and analcime ($2\theta = 16.08$, 18.38 and 26.12) were detected in the diffractogram of CaFZBFA. Diffraction peaks of zeolitic composites involving faujasite-Mg ($2\theta = 6.06^{o}$, 21.02^{o}, 26.64^{o} and 31.22^{o}) and sodalite ($2\theta = 13.98$, 19.78 and 82.44) were detected in MgFZBFA.

For the microwave alkaline hydrothermal products CaMZBFA and MgMZBFA, massive disappearance of the BFA hump can also be observed (Figures 3.13 and 3.14) but the diffraction peaks of silica, particularly those of cristobalites are still abundant in the diffractograms. This means that under the given experimental conditions, the amorphous glassy phases were thoroughly digested while some crystalline phases, particularly cristobalite have not been

digested completely. And they perchance become very obvious due to the dissolution and zeolitization of the more soluble amorphous glassy phases. The relative abundance of these SiO_2 diffraction peaks in the two diffractograms suggests that the microwave alkaline hydrothermal method for the zeolitization of the fly ash was less efficient as regards the dissolution of some crystalline SiO_2 phases than the fusion method. However, new and crystalline diffraction peaks were detected in the diffractograms of CaFZBFA and MgFZBFA, and this suggests some extent of transformations which have taken place. Some diffraction peaks of sodalite (2θ = 14.04°, 24.42°, 34.80°, 42.70°, 42.88° and 50.08°) and faujasite-Ca (2θ = 6.14°, 27.76°, 50.08°, 57.12° and 58.18°) were detected in the diffractogram of CaMZBFA. Diffraction peaks of chabazite-Mg (2θ = 9.4°, 13.98°, 15.92° and 80.38°) and sodalite (13.8°, 24.18°, 31.40°, 40.02° and 59.90°) were discovered in the diffractogram of MgMZBFA.

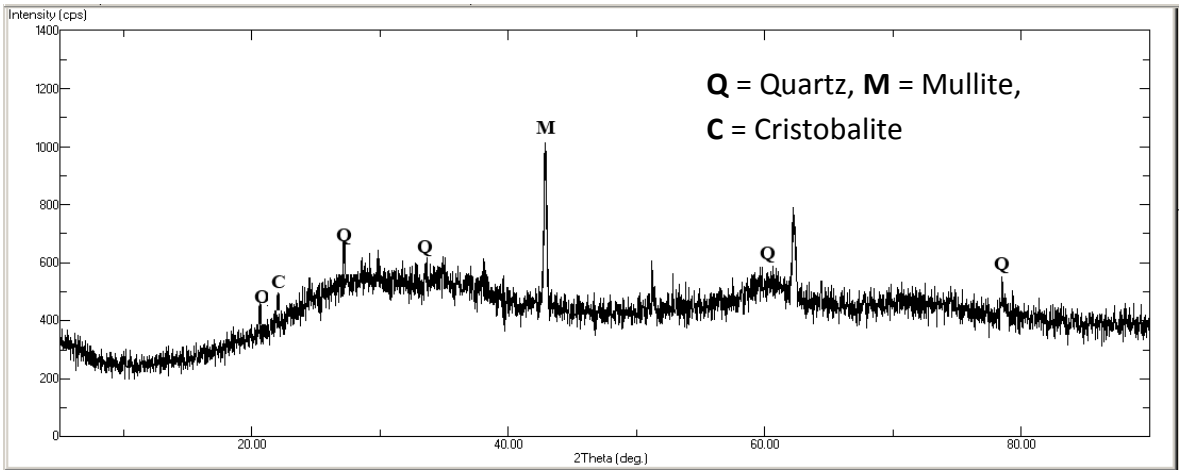

Figure 3.10 PXRD spectrum of BFA

The PXRD pattern of BFA exhibits glassy phase as an amorphous composition which is seen as broad hump at low 2θ angles. The glassy amorphous phase gradually decreases during zeolitic composite adsorbents formation.

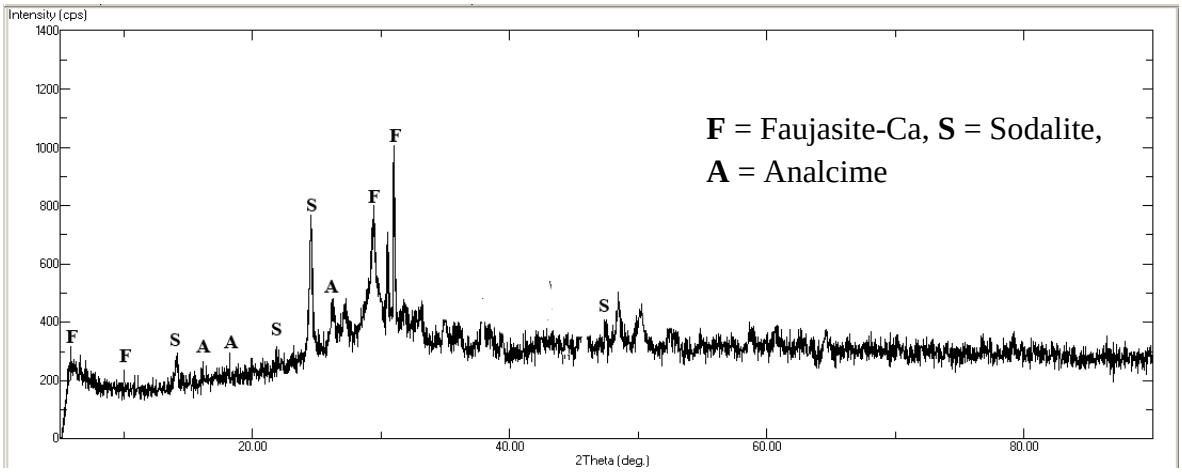

Figure 3.11 PXRD spectrum of CaFZBFA

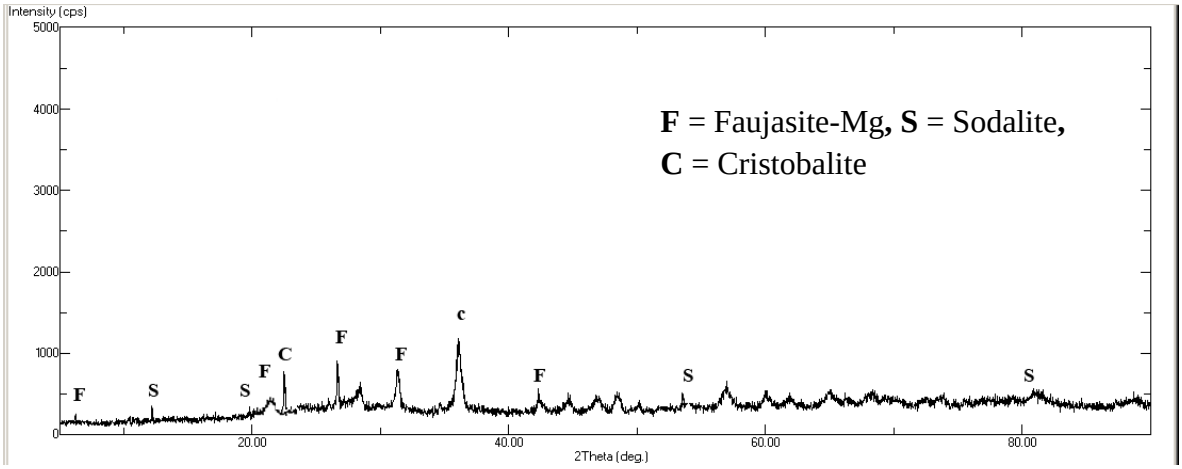

Figure 3.12 PXRD spectrum of MgFZBFA

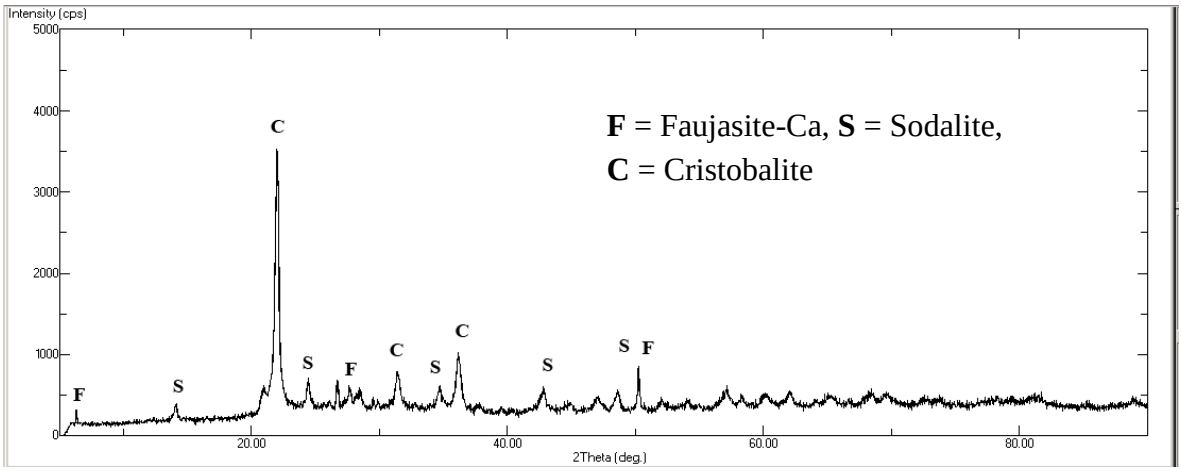

Figure 3.13 PXRD spectrum of CaMZBFA

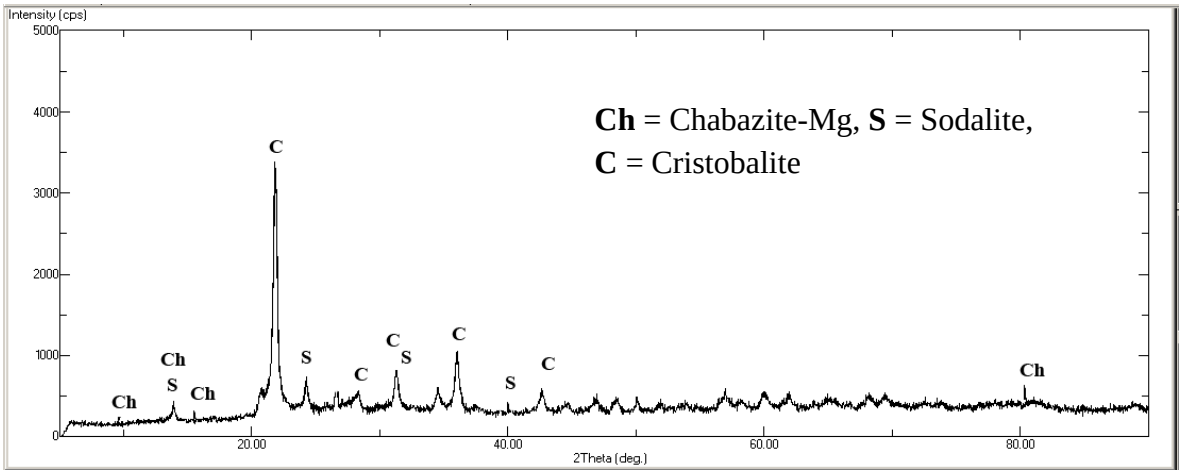

Figure 3.14 PXRD spectrum of MgMZBFA

❖ Scanning Electron Microscopy (SEM)

The transformations of the surface morphology of BFA through the zeolitization process were observed under a scanning electron microscope. SEM images of BFA, CaFZBFA, MgFZBFA, CaMZBFA and MgMZBFA were observed at ×2500 magnification. The particles of the BFA appear to be spherical (Figure 3.15a). The spherical appearance is as a result of cooling and solidification effect that the particles experience while being suspended in flue gases [12]. In the SEM micrographs that represent the fusion synthesis products CaFZBFA and MgFZBFA (Figure 3.15b and c), the particles appear to be in agglomerate form with rough morphologies, and the initial spherical shape of the BFA appears to be no more. This is due to the chemical impact involved in the zeolitization process [13], particularly the impact brought about by the alkali treatment of BFA which resulted in the dissolution of the mineral phases. For the microwave products CaMZBFA and MgMZBFA (Figure 3.15d and e), the development of rough, crystalline and non-spherical morphologies can also be observed. Porous nature of the products that could enhance their sorption abilities can also be seen from the micrographs.

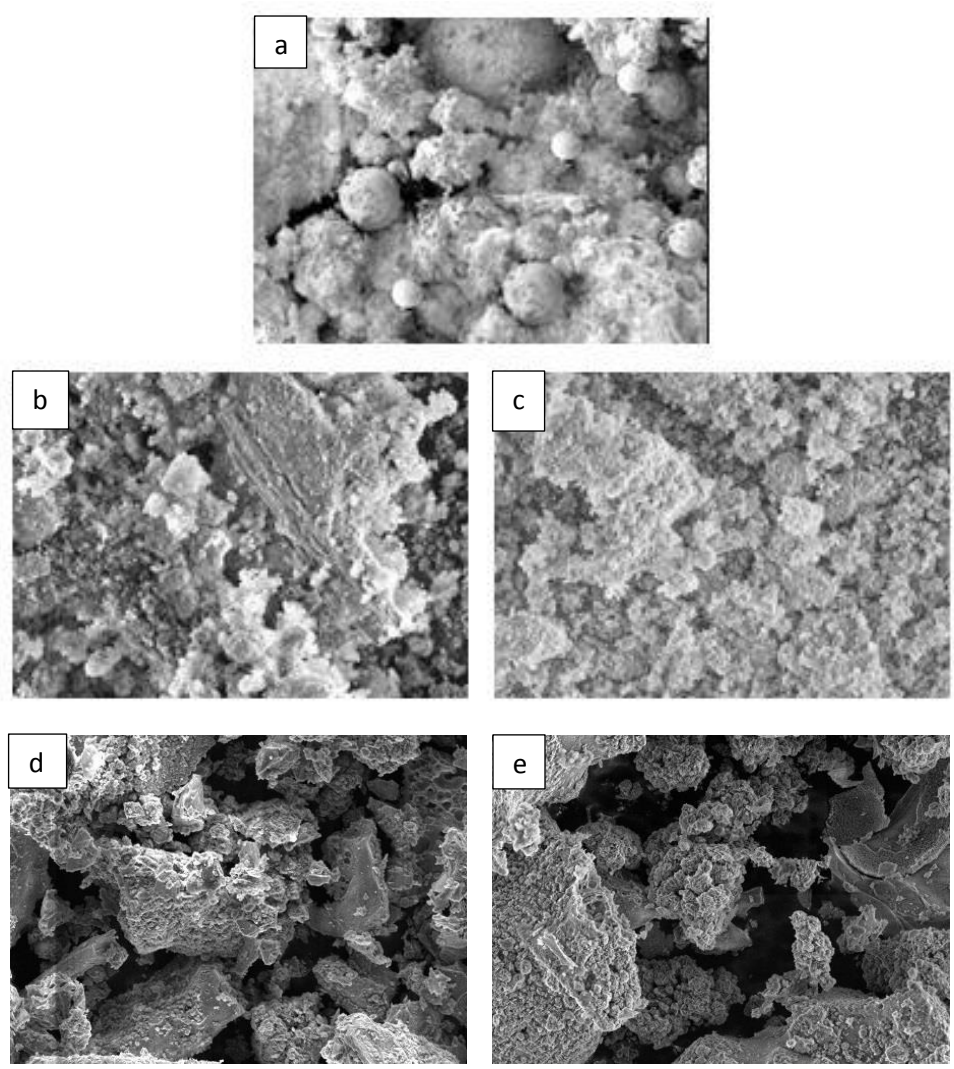

Figure 3.15 SEM micrographs at ×2500 magnification of (a) BFA
(b) CaFZBFA (c) MgFZBFA (d) CaMZBFA (e) MgMZBFA

The fusion products CaFZBFA and MgFZBFA appear to be less crystalline than the microwave alkaline hydrothermal products CaMZBFA and MgMZBFA. However, the particles of the fusion products appear puffy which could be an indication of the development of pore volumes. Furthermore, the fusion products, through SEM micrographs observation appear to be of greater surface areas than the microwave alkaline hydrothermal products.

REFERENCES

1. Cesareo, X-ray fluorescence spectrometry, in Ullmann's Encyclopedia of Industrial Chemistry. 2012, Wiley-VCH Verlag GmbH and Co: Weinheim, Germany.
2. Petiot, C. What is X-ray fluorescence. 2018 [cited 2018 1 September 2018]; Available from: https://hha.hitachi-hightech.com/en/blogs-events/blogs/2017/10/01/what-is-x-ray-fluorescence-xrf/.
3. Dutrow, B.L. and Clark, C.M. Geochemical instrumentation and analysis: X-ray powder diffraction (XRD). [cited 2018 11 September]; Available from: https://serc.carleton.edu/research_education/geochemsheets/techniques/XRD.html.
4. Petit, S. and Madejova, J., Fourier transform infrared spectroscopy, in Handbook of clay science. 2013, Elsevier Ltd.
5. Scanning electron microscopy. [cited 2018 14 September]; Available from: https://www.nanoscience.com/techniques/scanning-electron-microscopy/.
6. Scott, M.A., Kathleen, A.C., and Prabir, K.D., Handbook of zeolite science and technology. 2003, New York Marcel Dekker Inc. 1170.
7. Tantawy, M.A., El-Roudi, A.M., and Salem, A.A., Utilization of bagasse ash as supplementary cementitious material. International Journal of Engineering Research & Technology (IJERT), 2014. **3**(7).
8. Shah, B.A., Pandya, D.D., and Shah, H.A., Impounding of ortho-chlorophenol by zeolitic materials adapted from bagasse fly ash: Four factor three level box-behnken design modelling and optimization. Arab J Sci Eng, 2016.

9. Hildebrando, E.A., et al., Synthesis and characterization of zeolite NaP using kaolin waste as a source of silicon and aluminum. Materials Research, 2014.
10. Tanaka, H., Furusawa, S., and Hino, R., Synthesis, characterization, and formation process of Na-X zeolite from coal fly ash. Journal of Materials Synthesis and Processing, 2002. **10**(3): p. 143-148.
11. Wu, D.Y., et al., Synthesis of zeolite from thermally treated sediment. Ind. Eng. Chem. Res. , 2008. **47**(2): p. 295–302.
12. Musyoka, N.M., et al., Synthesis of zeolites from coal fly ash using mine waters. Minerals Engineering, 2013. **53**: p. 9–15.
13. Jha, B. and Singh, D.N., Flyash zeolites: Innovations, applications, and directions. Advanced Structured Materials, 2016. **78**: p. 5-31.